AGU100 ADVANCING EARTH AND SPACE SCIENCE

JGR

Journal of Geophysical Research: Atmospheres

RESEARCH ARTICLE
10.1029/2018JD028919

Key Points:
- Analysis of 21 automated weather stations (AWS) shows cloud radiative effects (CRE) highest at Summit, lowest at coasts
- MERRA-2, ERA-Interim, and CERES are consistent with AWS-derived CRE spatial distributions; ASR and CESM bias high in the south and northwest
- MERRA-2 agrees best with in situ measurements due to correct cloud radiation and good simulations of cloud properties and surface albedo

Supporting Information:
- Supporting Information S1
- Figure S1
- Figure S2
- Figure S3

Correspondence to:
W. Wang,
wenshanw@uci.edu

Citation:
Wang, W., Zender, C. S., van As, D., & Miller, N. B. (2019). Spatial distribution of melt season cloud radiative effects over Greenland: Evaluating satellite observations, reanalyses, and model simulations against in situ measurements. *Journal of Geophysical Research: Atmospheres*, *124*, 57–71. https://doi.org/10.1029/2018JD028919

Received 30 APR 2018
Accepted 4 DEC 2018
Accepted article online 15 DEC 2018
Published online 4 JAN 2019

Spatial Distribution of Melt Season Cloud Radiative Effects Over Greenland: Evaluating Satellite Observations, Reanalyses, and Model Simulations Against In Situ Measurements

Wenshan Wang[1], Charles S. Zender[1], Dirk van As[2], and Nathaniel B. Miller[3,4]

[1]Department of Earth System Science, University of California, Irvine, CA, USA, [2]Geological Survey of Denmark and Greenland (GEUS), Copenhagen, Denmark, [3]Cooperative Institute for Research in Environmental Science, University of Colorado Boulder, Boulder, CO, USA, [4]NOAA/Earth System Research Laboratory, Boulder, CO, USA

Abstract Arctic clouds can profoundly influence surface radiation and thus surface melt. Over Greenland, these cloud radiative effects (CRE) vary greatly with the diverse topography. To investigate the ability of assorted platforms to reproduce heterogeneous CRE, we evaluate CRE spatial distributions from a satellite product, reanalyses, and a global climate model against estimates from 21 automatic weather stations (AWS). Net CRE estimated from AWS generally decreases with elevation, forming a "warm center" distribution. CRE areal averages from the five large-scale data sets we analyze are all around 10 W/m^2. Modern-Era Retrospective Analysis for Research and Applications version 2 (MERRA-2), ERA-Interim, and Clouds and the Earth's Radiant Energy System (CERES) CRE estimates agree with AWS and reproduce the warm center distribution. However, the National Center for Atmospheric Research Arctic System Reanalysis (ASR) and the Community Earth System Model Large ENSemble Community Project (LENS) show strong warming in the south and northwest, forming a warm L-shape distribution. Discrepancies are mainly caused by longwave CRE in the accumulation zone. MERRA-2, ERA-Interim, and CERES successfully reproduce cloud fraction and its dominant positive influence on longwave CRE in this region. On the other hand, longwave CRE from ASR and LENS correlates strongly with ice water path instead of with cloud fraction or liquid water path. Moreover, ASR overestimates cloud fraction and LENS underestimates liquid water path substantially, both with limited spatial variability. MERRA-2 best captures the observed interstation changes, captures most of the observed cloud-radiation physics, and largely reproduces both albedo and cloud properties. The warm center CRE spatial distribution indicates that clouds enhance surface melt in the higher accumulation zone and reduce surface melt in the lower ablation zone.

1. Introduction

Cloud contributions to the surface energy budget are known to vary greatly over Greenland (Verlinde et al., 2016; Wang et al., 2018). Many large-scale gridded data sets such as satellite observations, reanalyses, and model simulations include the cloud and radiation fields necessary to determine cloud radiative effects (CRE) on large spatial scales. However, the accuracy and uncertainties in these CRE products are largely unknown because their CRE have not previously been systematically evaluated against in situ CRE estimates. Here we estimate the CRE spatial distribution from 21 automatic weather stations (AWS) over Greenland. CRE derived from AWS exhibits a telltale fingerprint reproduced by some but not all gridded CRE products. We use this fingerprint to evaluate cloud and radiation retrievals from five gridded data sets including one satellite observation, three reanalyses, and one global climate model. We then identify the most important factors that contribute to the verisimilitude of each gridded data set.

CRE, defined as the difference between all-sky and clear-sky surface radiation, is a "simple and effective" metric to assess cloud impacts on surface energy budget (Intrieri et al., 2002). Clouds warm surfaces through increased longwave radiation (i.e., positive CRE) and cool surfaces through the shortwave shading effect (i.e., negative CRE). The net effect, warming or cooling, strongly depends on location (Wang et al., 2018). In the high elevation accumulation zone of Greenland, clouds can augment surface heating caused by warm southerly advection, trigger massive surface melt (Bennartz et al., 2013), and enhance meltwater runoff (Van Tricht et al., 2016). In this region, the prevalent low-level liquid-containing clouds are optically thick enough to absorb longwave terrestrial radiation yet thin enough to transmit shortwave solar radiation (Bennartz et al., 2013; Cesana et al., 2012). Bright surface albedo in this region further suppresses the shortwave shading effect of clouds, due to less contrast between clouds and surfaces (Shupe & Intrieri, 2004). Clouds tend to cool the surface in the ablation zone, and an absence of clouds accelerates surface melt (Hofer et al., 2017; Kay & Gettelman, 2009). Ablation zone clouds are thicker (Zygmuntowska et al., 2012) and surfaces are darker (Perovich et al., 2002). The combination of these diverse surface and atmospheric conditions result in highly heterogeneous CRE in Greenland.

In the Arctic, gridded data sets are usually evaluated against short-term campaigns, sparse station measurements, or each other. For example, Cesana et al. (2015) and Liu and Key (2016) use cloud retrievals from active sensors to evaluate reanalyses and model simulations. However, active sensor retrievals can only be cross-validated at Summit, the sole station with comprehensive cloud measurements inside Greenland (Lacour et al., 2017; Shupe, Turner, et al., 2013).

To our knowledge, Van Tricht et al. (2016) is the only prior study that explicitly presents a spatial distribution of CRE over most of Greenland. They estimated CRE distribution using 1 month of data from each season in 2010 from the CloudSAT-CALIPSO (Cloud-Aerosol Lidar and Infrared Pathfinder Satellite Observation) products. They conclude that clouds warm the southern and northwestern coasts the most, and the northern interior the least, strongly correlated with cloud water path. Although the active sensors onboard CALIPSO provide more accurate instantaneous observations of clouds, especially the prevalent low-level clouds in the Arctic, compared to passive sensors (Cesana & Chepfer, 2012; Chan & Comiso, 2013; Henderson et al., 2013; Kay & L'Ecuyer, 2013), they have difficulty capturing the climatological cloud effects due to their limited spatial-temporal sampling (Kay & L'Ecuyer, 2013; Liu, 2015). At the southern and western coasts where surface melts frequently in summer (Hall et al., 2009), surface albedo rather than cloud properties might play a more important role in determining CRE (Wang et al., 2018).

In this study, we evaluate CRE spatial distributions from five well-known gridded data sets against estimates from 21 in situ AWS during the melt seasons from 2008 to 2013. The five data sets include one satellite product, the Clouds and the Earth's Radiant Energy System (CERES); two global reanalyses, the Modern-Era Retrospective Analysis for Research and Applications, version 2 (MERRA-2), and the European Centre for Medium-Range Weather Forecasts Interim reanalysis data (ERA-Interim); one regional reanalysis, the Arctic System Reanalysis (ASR); and one global climate model, the Community Earth System Model (CESM) Large Ensemble Project (LENS). We explain the discrepancies in terms of physical properties relevant to cloud-surface-radiation interactions that determine CRE. Section 2 describes the data and methods we use to estimate CRE and perform comparisons. Section 3 presents CRE spatial distribution estimated from AWS. Section 4 evaluates CRE spatial distributions from gridded data sets against the interpolated maps and interstation changes of in situ measurements. Section 5 examines the gridded data sets' cloud-radiation physics and evaluates their retrieval of major CRE factors against observations. In section 6, we discuss the shortcomings of CALIPSO retrievals to reveal climatological CRE. Section 7 summarizes the main findings of this study and their implications.

2. Data and Method

We examine five gridded data sets that provide both all-sky and clear-sky surface radiation fields at high spatial resolution. We focus on the melt seasons here defined as May to August from 2008 to 2013 since there are not enough clear days in September needed to remove insolation bias caused by station tilt (Wang et al., 2016).

CERES cloud retrievals integrate Moderate Resolution Imaging Spectroradiometer-observed radiance with an emphasis on radiative issues (Wielicki et al., 1996). CERES retrieves cloud top properties and estimates cloud base height based on empirical formulas. We use their monthly Synoptic Radiative Fluxes and Clouds (SYN) Edition-3A Level-3 data with a spatial resolution of 1°. MERRA reanalyses take advantage of numerous satellite measurements. MERRA-2, a successor of MERRA, uses an updated Goddard Earth Observing System model and assimilates more types of observations (Gelaro et al., 2017). Its monthly cloud and radiation retrievals are in grids of 1/2° latitude and 2/3° longitude. ERA-Interim is the latest global reanalysis from the European Centre for Medium-Range Weather Forecasts (ECMWF; Dee et al., 2011), which also assimilates both in situ and satellite observations and uses forecast models to predict cloud properties. It is often employed to drive

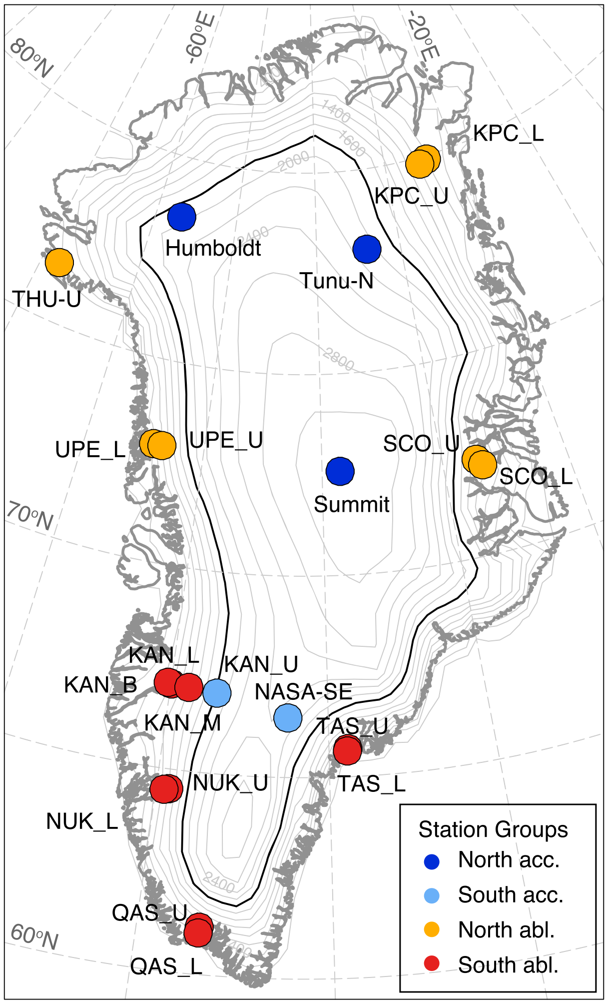

Figure 1. Positions of weather stations used in this study with highlighted isoline of 1,800 m. Stations in the northern accumulation zone are represented in dark blue, southern accumulation zone in light blue, northern ablation zone in yellow, and southern ablation zone in red. abl = ablation zone; acc = accumulation zone.

regional models in the Arctic (Fettweis et al., 2017; Noël et al., 2015; Wesslén et al., 2014). The spatial resolution is ~0.7°. ASR is a high-resolution regional reanalysis focused on the Arctic (Wesslén et al., 2014). It uses the High-Resolution Land Data Assimilation system and the Polar Weather Forecast Model as the forecast model. The highest spatial resolution of ASR is 15 km. In this study, we use ASR 30-km products and regrid to MERRA-2 rectilinear grids using bilinear interpolation. LENS consists of 40 ensemble members from simulations of the fully coupled CESM, including diagnostic ocean biogeochemistry and the atmospheric carbon dioxide cycle (Kay et al., 2015). The large-ensemble means reduce the influence of internal climate variabilities. We utilize the LENS RCP8.5 scenario. This closely mimics historical radiative forcing (Sanford et al., 2014) and has a spatial resolution of ~1°.

All 39 AWS from the Greenland Climate Network (GC-Net; Steffen et al., 1996) and the Programme for Monitoring of the Greenland Ice Sheet (PROMICE; van As & Fausto, 2011) by 2013 have gone through rigorous data quality control to reduce interference from the typical problems experienced by unattended weather stations, including station tilt, low cosine response at large solar zenith angle, riming on sensor domes, and sensor overheating (see details of data quality control and instrument uncertainties in section 2 in Wang et al., 2018). Twenty-one stations with at least one complete year of high-quality data remain (Figure 1 and Table S1 in the supporting information), among which four are from GC-Net, all in the accumulation zone (elevation ≥1,800 m); the rest are from PROMICE, with one station in the accumulation zone. In the ablation zone (elevation < 1,800 m), PROMICE stations usually operate in pairs along one glacier (e.g., two stations near Nuuk). Stations suffixed with "U" and "L" are in the upper (e.g., NUK_U) and lower (e.g., NUK_L) ablation zones, separately. We describe stations in the north of 70°N as northern stations and south of 70°N as southern stations.

Same as in Intrieri et al. (2002), we define CRE as the difference between all-sky and clear-sky surface radiation. AWS measure all-sky surface radiation. Clear-sky radiation is simulated using the Column Radiation Model (Zender, 1999) driven by the Level-3 Atmospheric Infrared Sounder, AIRS (AIRS Science Team/Joao Texeira, 2013). The uncertainty of clear-sky simulations is less than 10 W/m^2 (Wang et al., 2018).

CERES, MERRA-2, ERA-Interim, and LENS provide both total cloud fraction and low-level cloud fraction. ASR provides only the vertical profiles of cloud fraction. MERRA-2 and ERA-Interim define low-level clouds based on cloud height from the ground. CERES and LENS define low-level clouds as clouds below 700 hPa. In Greenland, the latter definition is problematic due to the generally high elevations there. For example, at Summit, the surface pressure is often lower than 700 hPa. Since LENS also provides vertical profiles of cloud fraction, we calculate the total and low-level cloud fraction for LENS and ASR. Following ERA-Interim's definition (European Centre for Medium-Range Weather Forecasts, 2018), we categorize cloud layers as low level if the layer/surface pressure ratio is greater than 0.8, as midlevel if the ratio is greater than 0.45 and less than 0.8, and as high level if less than 0.45. Then we use the maximum-random overlap assumption same as the other four data sets to calculate total cloud fraction (Zib et al., 2012, and personal communication with Dr. Michael G. Bosilovich from National Aeronautics and Space Administration in February 2018). Clouds of the same height level are assumed to be maximally overlapped. Different cloud height levels are assumed to be randomly overlapped.

To evaluate cloud fraction and liquid water path (LWP) from the gridded data sets, we use data from the Integrated Characterization of Energy, Clouds, Atmospheric State, and Precipitation at Summit (ICECAPS), the only multiyear comprehensive in situ cloud observations in Greenland (Shupe, Turner, et al., 2013). ICECAPS retrieves cloud fraction and LWP using multiple instruments. Miller et al. (2015) estimate cloud fraction using

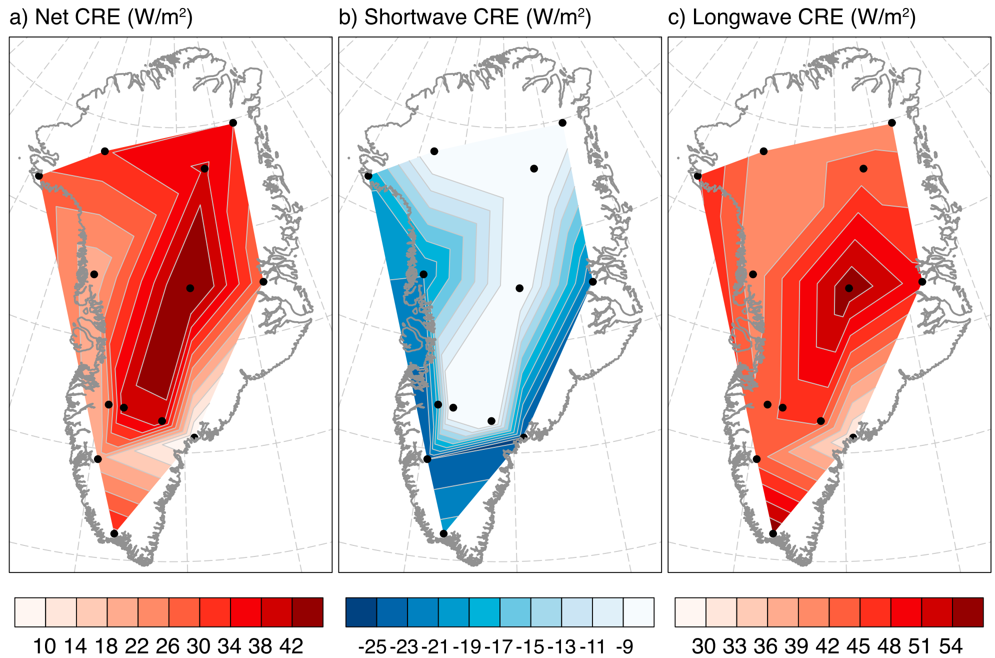

Figure 2. Interpolated (a) net CRE, (b) shortwave CRE, and (c) longwave CRE from automatic weather stations (black dots) in the accumulation and upper ablation zone. CRE = cloud radiative effects.

the temporal average of cloud presence detected by Vaisala ceilometer, millimeter cloud radar, and MicroPulse Lidar. Due to the narrow viewing angles of these instruments, this type of cloud fraction might be significantly different from those based on whole sky images (e.g., human and satellite observations), especially when the air is stagnant (Qian et al., 2012). LWP is derived from the Humidity and Temperature Profiler microwave radiometer and a second high-frequency microwave radiometer (Turner et al., 2007), with an uncertainty of $\sim$3 g/m^2.

3. CRE Spatial Distribution From In Situ Measurements

We interpolate CRE estimates from the 21 weather stations to maps to demonstrate the spatial distribution of CRE. Steep slopes near the coasts render large-scale maps of the entire Greenland insufficient to present the large spatial variability in the ablation zone. Therefore, the interpolated maps show only stations in the accumulation zone and in the upper ablation zone. We then use 2-D plots of latitude-elevation and latitude-albedo to show CRE variability in the ablation zone.

CRE generally decreases with elevation during the melt season (Figure 2a). It is highest at Summit and lowest near coasts. Shortwave cooling by clouds is weakest near Summit due to the constantly high albedo. Longwave warming is strongest there probably due to the dry atmosphere and prevalent low-level liquid-containing clouds (Lacour et al., 2017; Miller et al., 2015; Shupe, Turner, et al., 2013). These clouds most likely form by orographic lifting during warm southerly advection (Zygmuntowska et al., 2012) and are usually decoupled from the surface (Curry et al., 1996; Shupe, Persson, et al., 2013; Tjernström et al., 2014) as the boundary layer is drier at higher elevations. As elevation decreases so does albedo, and shortwave CRE strengthens from Summit to the coasts (Figure 2b). The only exception is QAS_U (the southernmost station at 900 m), where albedo is abnormally high (0.67) for its latitude and relative to albedos from nearby stations QAS_L (0.34 at 280 m) and NUK_U (0.64 at 1,120 m) because QAS_U usually receives a lot more snowfall than most other upper stations (U stations). As elevation decreases, longwave CRE first decreases until near the equilibrium line and then increases (Figure 2c). This stronger warming effect near coasts might be caused by an increasing cloud fraction, formed mostly by marine stratus clouds (Walsh et al., 2009). However, on the southeastern coast next to relatively warm Atlantic water (Station TAS), there is no increased warming effect. Due to the persistent anticyclonic conditions and katabatic winds over Greenland, this area is more likely dominated by the cold northerly air advection than by the warm ocean circulation (Hanna et al., 2014). Nevertheless, between the two neighboring PROMICE stations at TAS, the lower station, TAS_L, has a higher

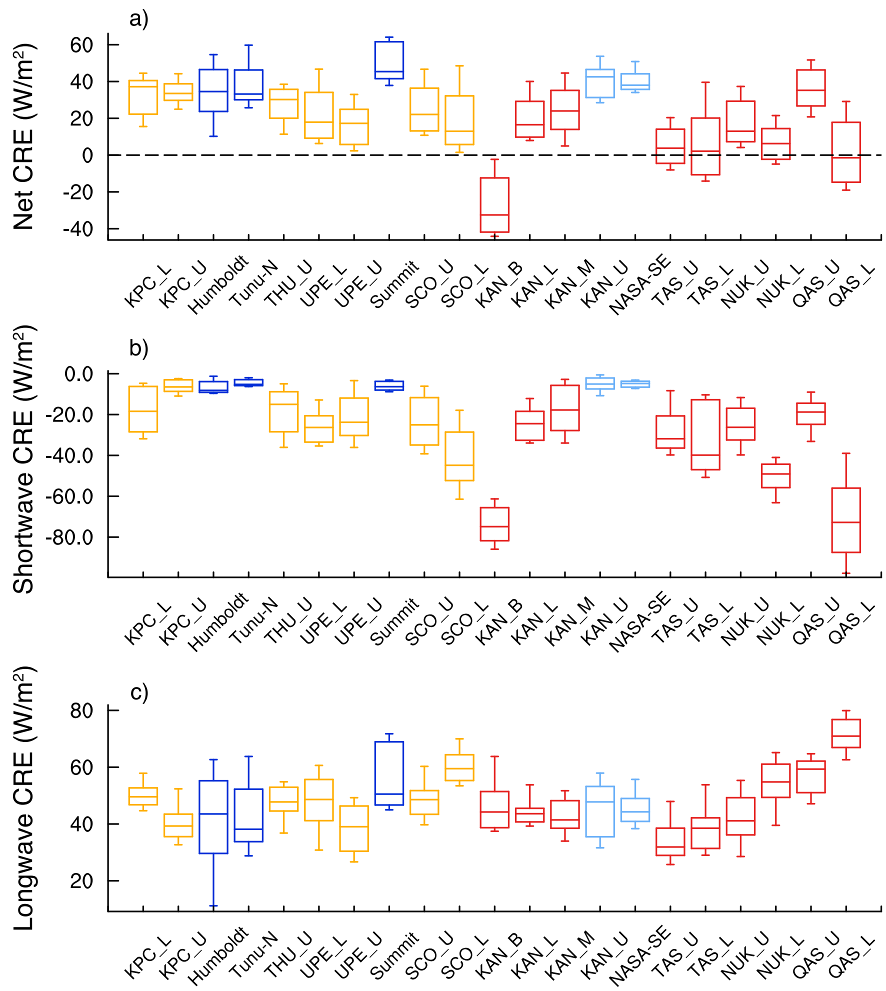

Figure 3. Statistics of 20-day running average (a) net CRE, (b) shortwave CRE, and (c) longwave CRE at each weather station. Whiskers show lower decile and upper decile, and box lines show upper quartile, median, and lower quartile. Station colors are as in Figure 1. CRE = cloud radiative effects.

longwave CRE than the upper station, TAS_U, demonstrating a larger warming effect at lower elevations (Figure 3c). Net CRE, the sum of shortwave and longwave CRE, decreases monotonically from Summit to the coasts.

To interpolate CRE estimates from stations to maps, we first use the Delaunay triangulation method to generate convex hulls enclosing the station data to project them to a triangular-meshed map and then smooth the map using cubic spline interpolation. This method does not extrapolate and connects all stations to their nearest neighbors to form the triangular mesh. We compare this result with results from three other commonly used spatial interpolation methods: the tension spline, the natural neighbor, and the nearest distance interpolation (Figure S1). Due to the limited number of stations and their heterogeneous distribution, the absolute values are subject to large uncertainties. However, the spatial pattern of CRE decreasing with elevation remains unchanged.

This CRE spatial distribution is robust throughout the whole melt season (Figure 3). The statistics of 20-day running average CRE (smoothing in order to remove synoptic influences) also show decreasing values from the accumulation zone (dark and light blue boxes in Figure 3a) to the ablation zone (yellow and red boxes in Figure 3a), with the highest at Summit. Shortwave CRE strengthens from high to low elevation (Figure 3b). Longwave CRE decreases from Summit to near the equilibrium line and then increases seaward (Figure 3c).

To better resolve the ablation zone, we scatterplot CRE with respect to latitude and elevation (Figures 4a–4c). Net CRE is smaller at lower latitudes and elevations (Figure 4a), mostly due to strong negative shortwave CRE

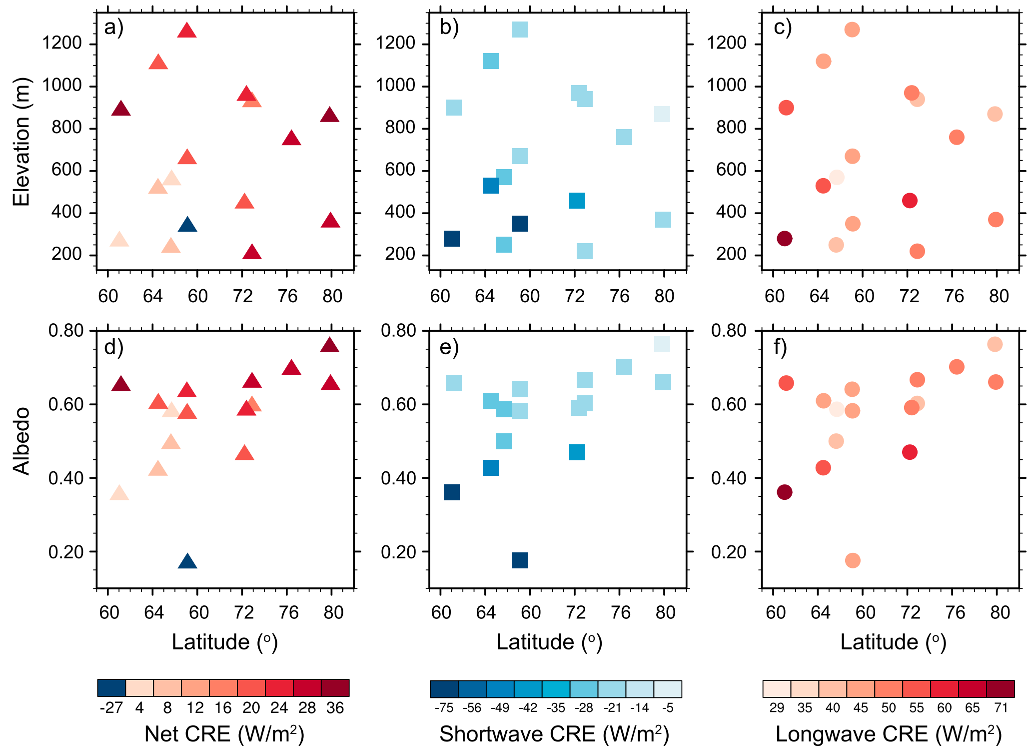

Figure 4. Ablation zone net CRE (a and d), shortwave CRE (b and e), and longwave CRE (c and f) in scatterplots of latitude elevation (a–c), and latitude albedo (d–f). CRE = cloud radiative effects.

in this quadrant (Figure 4b). The longwave CRE distribution is more scattered with slightly higher values at lower elevations (Figure 4c). In the scatterplot of latitude and albedo (Figures 4d–4f), net CRE is better aligned. Net CRE decreases from high albedo to low albedo, similar to shortwave CRE (Figures 4d and 4e). Therefore, in the ablation zone, albedo governs the spatial distribution of CRE. Although albedo generally decreases with latitude and elevation, the local conditions, for example, tundra at KAN_B, can also exert a substantial influence.

In summary, net CRE over Greenland presents a "warm center" spatial pattern: peaking at Summit and decreasing toward the coasts. Shortwave CRE decreases with elevation, largely due to albedo. Longwave CRE increases away from the equilibrium line, both inland and coastward, probably due to increased cloudiness in those areas and the dry atmosphere at high elevations.

4. Evaluating CRE Spatial Distributions From Gridded Data Sets Against In Situ Measurements

4.1. CRE MAPS

CRE areal averages from the five gridded data sets we compare are similar (numbers above each panel in Figure 5). However, their spatial distributions present two distinct patterns: warm center and warm L-shape (i.e., warming in the south and northwest). CRE estimated from MERRA-2, ERA-Interim, and CERES generally decrease with elevation (the warm center pattern). The highest values are near Summit with a second maximum in the South Dome area. Low values predominate along the coasts with the lowest values in the west. ASR and LENS show relatively large positive CRE in the south and northwest (the warm L-shape pattern). Although the strongest negative CRE are also in the western ablation zone, the positive CRE are smallest in the northeast and increase toward the west and south in the accumulation zone.

Most inter-data set discrepancies stem from longwave CRE differences in the accumulation zone. Shortwave CRE spatial distributions from different data sets are similar: Weak cooling effects with small variability in the accumulation zone and stronger cooling as elevation decreases (Figure S2). Longwave CRE from the warm center group (MERRA-2, ERA-Interim, and CERES) are largest at Summit and along the coasts (Figure 6), consistent with Cox et al. (2014). Longwave CRE from the warm L-shape group (ASR and LENS) are larger in the

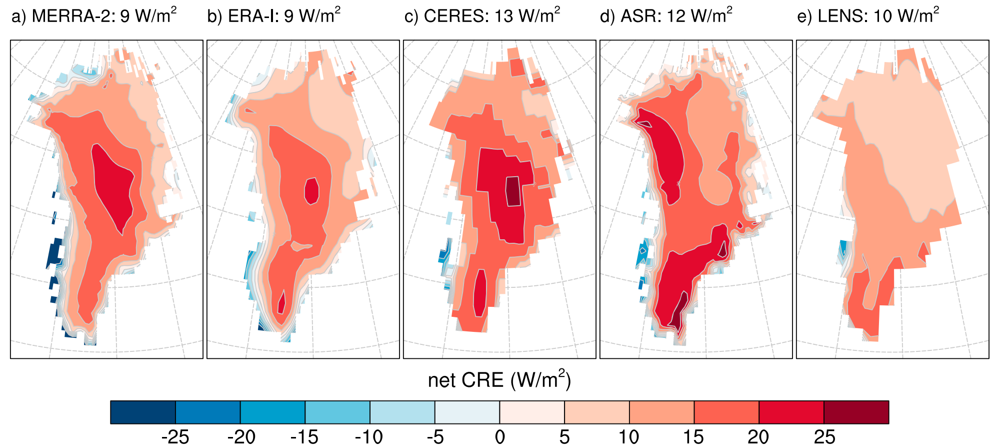

Figure 5. Net CRE from (a) MERRA-2, (b) ERA-Interim, (c) CERES, (d) ASR, and (e) LENS. Numbers above panels are areal averages. MERRA = Modern-Era Retrospective Analysis for Research and Applications; CERES = Clouds and the Earth's Radiant Energy System; ASR = Arctic System Reanalysis; LENS = Large ENSemble Community Project; CRE = cloud radiative effects.

south. ASR also shows strong warming in the northwest. To compare spatial distributions quantitatively, we interpolate the other four onto the LENS grid (one of the coarsest spatial resolutions) and calculate their pattern correlations (Tables S2 and S3). Shortwave CRE from all data sets are generally well correlated with one another. The correlation coefficients are around 0.8 in the ablation zone and greater than 0.5 in the accumulation zone. As for longwave CRE, only data sets in the same warm pattern group are well correlated. Correlation coefficients of data sets from different warm pattern groups are mostly around 0.3. The value is lower in the accumulation zone than in the ablation zone. Therefore, longwave CRE in the accumulation zone leads to the most inter-data set discrepancies in CRE spatial distribution.

4.2. CRE Interstation Changes

Section 4.1 evaluates data sets in terms of CRE large-scale spatial patterns. In this section, we evaluate data sets in their closest grid cell against in situ measurements at each weather station (distances between stations and grid cells are listed in Table S1). Although temporal averaging can mitigate interplatform differences (e.g., footprint size and instrument sensitivity), values from in situ measurements, remote sensing products, and model simulations are never the same (Li & Trishchenko, 2001). Therefore, we focus on the relative changes between stations rather than on the absolute differences and on relatively large interstation changes since the interstation variabilities from gridded data sets are inherently smaller than that of station observations due to the larger footprint.

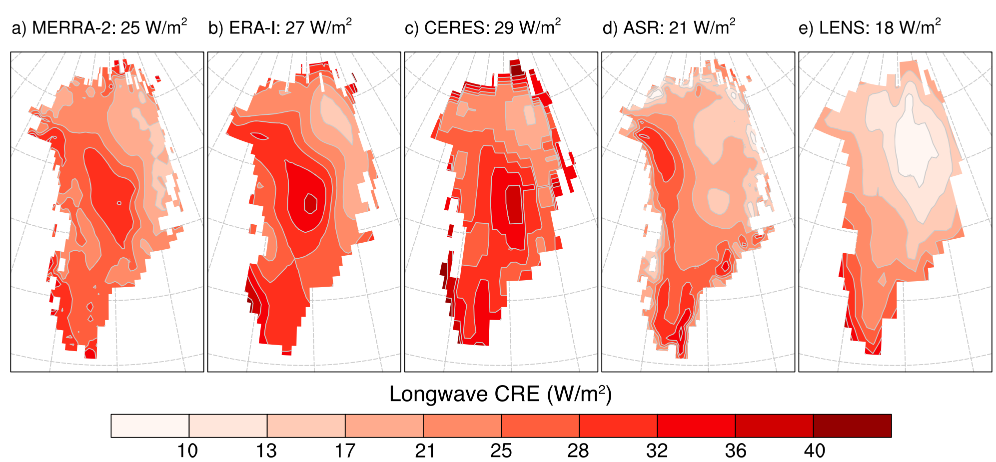

Figure 6. Same as Figure 5 but for longwave CRE.

10.1029/2018JD028919

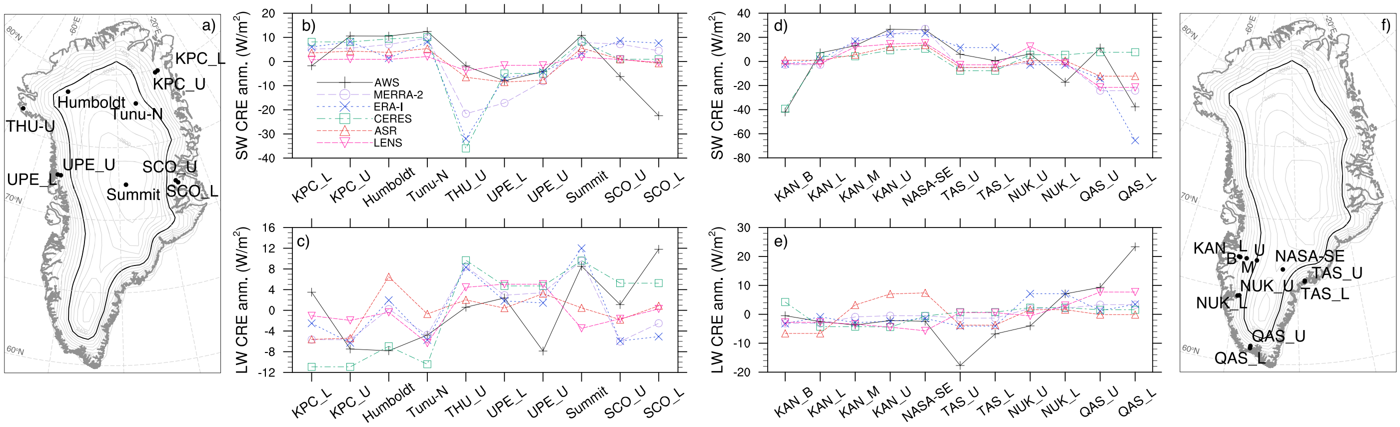

Figure 7. Station anomalies of (b) shortwave CRE in the north, (d) shortwave CRE in the south, (c) longwave CRE in the north, and (e) longwave CRE in the south from weather stations (black lines with pluses), MERRA-2 (purple lines with circles), ERA-Interim (blue lines with crosses), CERES (green lines with rectangles), ASR (red lines with uppointing triangles), and LENS (pink lines with downpointing triangles). (a) Positions of the northern stations used in (b) and (c). (f) Positions of the southern stations used in (d) and (e). CRE = cloud radiative effects; AWS = automatic weather stations; MERRA = Modern-Era Retrospective Analysis for Research and Applications; CERES = Clouds and the Earth's Radiant Energy System; ASR = Arctic System Reanalysis; LENS = Large ENSemble Community Project.

Shortwave CRE from all gridded data sets successfully reproduce the major transitions between the ablation and accumulation zones, but not changes inside the ablation zone with steeper slopes (Figures 7b and 7d). In the north (Figure 7b), all gridded data sets show decreasing shortwave CRE from Tunu-N down to UPE and increasing shortwave CRE back up to Summit, as in the in situ observation. However, on the eastern side, from Summit to SCO, most gridded data sets only show a slightly decreasing trend. ERA-Interim even shows an increasing trend. In the ablation zone, no gridded data set shows a lower value at the lower stations between the station pairs (e.g., KPC_U vs. KPC_L). Moreover, CERES, ERA-Interim, and MERRA-2 overestimate the difference between THU with Tunu-N and UPE to different degrees. In the south (Figure 7d), all gridded data sets capture the trends from KAN_L to TAS_U (Figure 7d). CERES closely matches observations between KAN_B and KAN_L on the western side of Greenland, yet it flattens out through the southern coasts. By contrast, ERA-Interim shows better results at the southernmost coasts but not in the west.

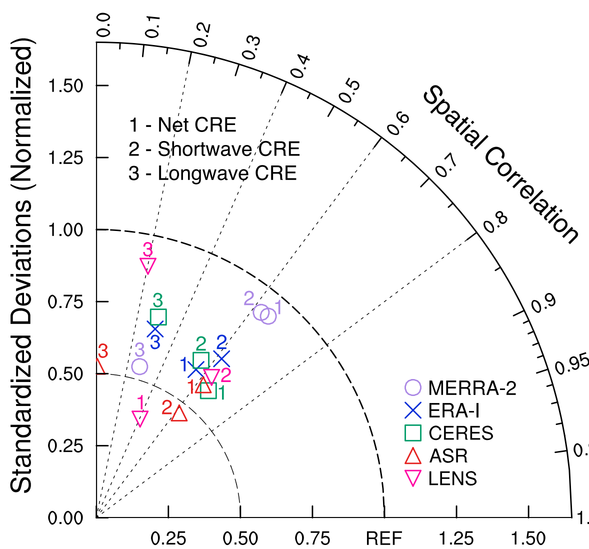

Figure 8. Spatial correlations and normalized standard deviations of (1) net CRE, (2) shortwave CRE, and (3) longwave CRE estimated from the five gridded data sets (colors and markers same as in Figure 7) comparing with in situ observations. CRE = cloud radiative effects; MERRA = Modern-Era Retrospective Analysis for Research and Applications; CERES = Clouds and the Earth's Radiant Energy System; ASR = Arctic System Reanalysis; LENS = Large ENSemble Community Project.

Resemblance of longwave CRE from the gridded data sets to in situ observations is worse than shortwave CRE (Figures 7c and 7e). In the north (Figure 7c), although the warm center group of data sets reproduces the relatively strong warming effects at Summit, they overestimate the spatial variability in the northernmost area (between KPC, Humboldt, and THU; Figure 7c). The warm L-shape group completely misses the "warm center and warm coasts" spatial features from in situ measurements. In the south (Figure 7e), the gridded data sets underestimate the overall spatial variability. None of them reproduce the large increasing trend from NUK_U to QAS_L (Figure 7e).

Although spatial resolutions and distances between certain AWS and grid cells vary among the five gridded data sets (Table S1), higher resolutions (e.g., MERRA-2) and shorter distances (e.g., MERRA-2 and ASR at QAS_L) do not improve the agreement between gridded and AWS CRE changes. Our comparisons focus on the interstation changes over a relatively long distance, where data set resolutions and distances between stations and grid cells are not critical factors.

The Taylor diagram summarizes the spatial variabilities of the gridded data sets and the in situ station measurements, as well as correlations between them (Figure 8). Since absolute values are not in the scope of this study, we do not include root-mean-square difference circles in the figure. With a high correlation and a similar variability, net CRE from MERRA-2 most

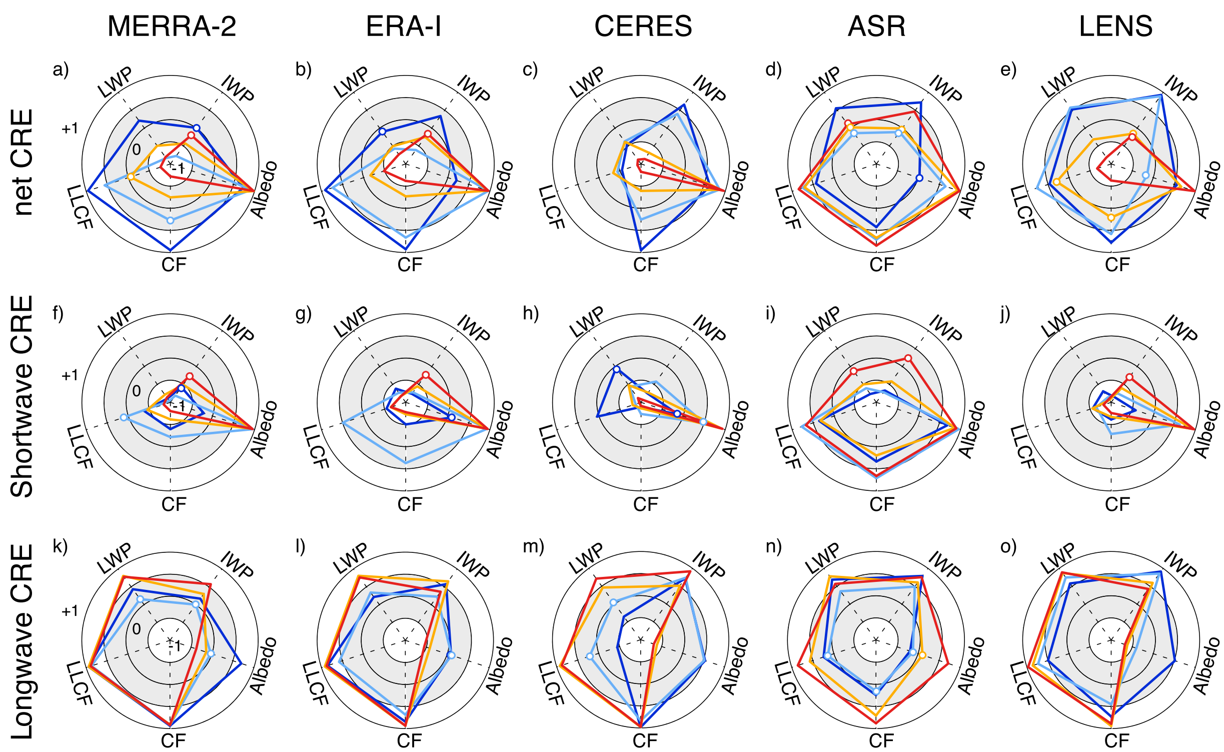

Figure 9. Correlations of CRE major factors (cloud fraction, low-level cloud fraction, liquid water path, ice water path, and surface albedo) with net CRE (a–e), shortwave CRE (f–j), and longwave CRE (k–o) from the five gridded data sets (each represented in one column). Colors represent different regions defined the same as in Figure 1. Insignificant correlations are marked by hollow circles. CRE = cloud radiative effects; LWP = liquid water path; IWP = ice water path; LLCF = low-level cloud fraction; CF = cloud fraction; CERES = Clouds and the Earth's Radiant Energy System; ASR = Arctic System Reanalysis; LENS = Large ENSemble Community Project.

closely resembles in situ observations. It produces the best shortwave CRE and fair longwave CRE. Net CRE from CERES, ASR, and ERA-Interim also correlate relatively well with observations; however, their spatial variabilities are small (around half of the reference). The global climate model, LENS, with fully prognostic clouds and environmental conditions, presents the worst resemblance. Overall, shortwave CRE is better represented in the gridded data sets than longwave CRE, among which ASR shows almost zero correlation with observations.

5. Examining Model Cloud-Radiation Physics and Estimates of CRE Factors

In this section, we examine the cloud-radiation relationships in radiative transfer physics of the five data sets, as well as evaluate the major factors determining CRE against in situ observations where possible.

The net effects of clouds on surface energy budget result from a complex synthesis of cloud macrophysics properties (cloud fraction and water path), cloud microphysics properties (cloud phase and particle size), and environmental conditions (surface albedo in melt season; Arking, 1991; Cox et al., 2015; Curry et al., 1996; Shupe & Intrieri, 2004; Verlinde et al., 2016). According to in situ observations, net CRE during melt seasons is largely determined by its shortwave component in the ablation zone and by longwave CRE in the accumulation zone (Wang et al., 2018). Albedo dominates the spatial variability of shortwave CRE in the ablation zone (Shupe & Intrieri, 2004). Cloud fraction and LWP contribute negatively to CRE and are major influences in the accumulation zone (Shupe & Intrieri, 2004). The responses of longwave CRE to major CRE factors are more complicated. Cloud fraction, mostly low-level cloud fraction, is the primary influence (Bennartz et al., 2013; Qian et al., 2012; Shupe & Intrieri, 2004; Walsh et al., 2009). LWP also contributes significantly (Shupe & Intrieri, 2004), even at Summit (Bennartz et al., 2013; Miller et al., 2015; Shupe, Turner, et al., 2013).

The quality of CRE estimates depends not only on obtaining the accurate quantities of these cloud and environmental properties but also on reproducing their interactions. All the platforms, satellites, reanalyses, and models use their own radiation transfer models to estimate surface radiative fluxes (Geier et al., 2003;

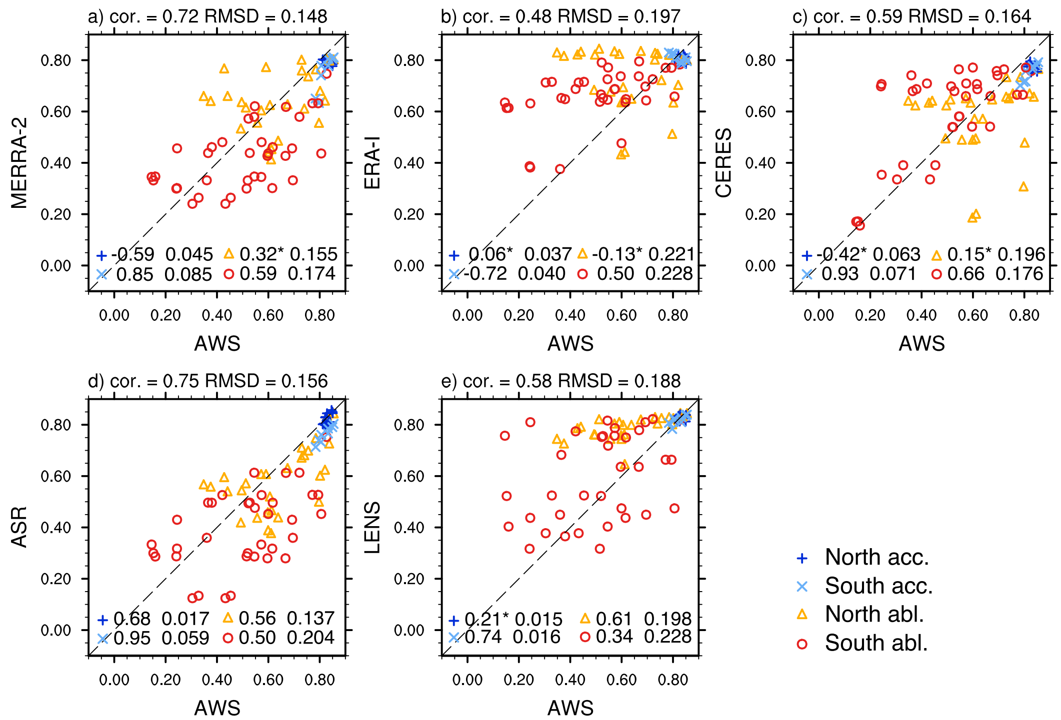

Figure 10. Monthly albedo averaged over 2008–2013 from (a) MERRA-2, (b) ERA-Interim, (c) CERES, (d) ASR, and (e) LENS against weather stations. Colors represent different regions defined as in Figure 1. The two numbers above each panel are correlation coefficient and RMSD for all stations. The two columns of numbers inside panels are correlation coefficient and RMSD for each region. Insignificant results are marked by asterisks. MERRA = Modern-Era Retrospective Analysis for Research and Applications; RMSD = root-mean-square difference; CERES = Clouds and the Earth's Radiant Energy System; AWS = automatic weather stations; ASR = Arctic System Reanalysis.

Walsh et al., 2009; Wielicki et al., 1996). Satellite products use remote sensed cloud properties and atmospheric and surface conditions to diagnose cloud radiative characteristics. Reanalyses forecast cloud properties based on assimilated atmospheric and surface conditions (Walsh et al., 2009). Fully coupled climate models simulate both clouds and environmental conditions.

To evaluate the cloud-radiation physics, we count total cloud fraction, low-level cloud fraction, cloud water path (both liquid and ice), and surface albedo as major CRE factors. For each CRE component (shortwave, longwave, and net), we calculate its pattern correlation with these major CRE factors and present them on a polar coordinate using radii. The stronger the correlations, the more similar the spatial distributions (Figure 9).

Cloud-radiation physics in MERRA-2, ERA-Interim, and CERES are generally consistent with current understandings summarized above. LENS captures most of the features, especially in shortwave. ASR differs in several ways. In MERRA-2, ERA-Interim, CERES, and LENS, net CRE in the southern ablation zone (red lines in the top row panels) is mainly determined by shortwave CRE (middle row). Net CRE in the northern accumulation zone (dark blue lines in the top row panels) is mainly determined by longwave CRE (bottom row). The northern ablation (yellow lines) and southern accumulation zones (light blue lines) are transitions between these two types. In these four data sets, shortwave CRE strongly correlates with albedo except in the northern accumulation zone. Cloud fraction and LWP exhibit negative influences in the ablation zones. In MERRA-2, ERA-Interim, and LENS, the negative influences from LWP are stronger; in CERES, those from cloud fraction are stronger, consistent with findings using sensitivity analysis in Huang et al. (2017). The striking differences stem from longwave CRE in the accumulation zones (blue lines in the bottom row panels). Agreeing with observations, longwave CRE from MERRA-2 and ERA-Interim are dominated by cloud fraction, especially low-level cloud fraction. However, none of them shows a distinguishably stronger correlation with LWP than with ice water path. Correlations between albedo and longwave CRE are more likely to be concurrent events rather than causal links. In CERES, the weak correlation with low-level cloud fraction might be caused by its

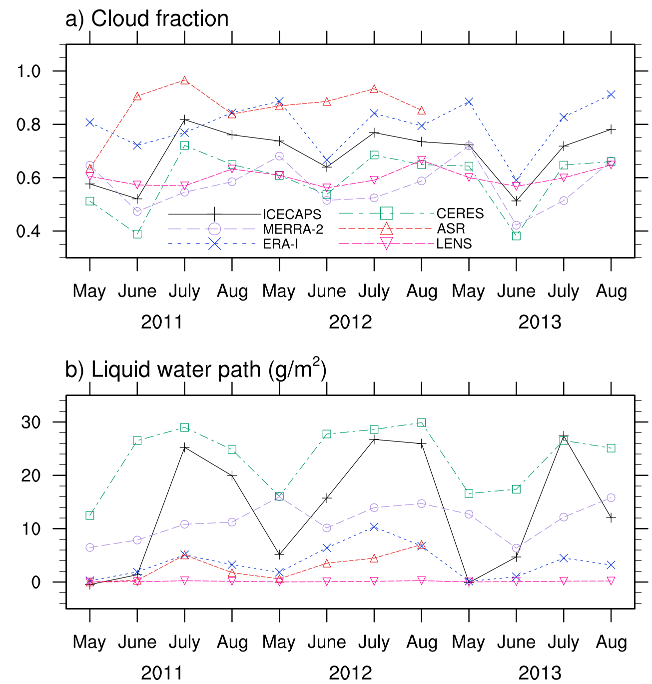

Figure 11. Cloud fraction and liquid water path from in situ observations and the five gridded data sets at Summit in melt seasons from 2011 to 2013. Symbols are the same as in Figure 7. ICECAPS = Integrated Characterization of Energy, Clouds, Atmospheric State, and Precipitation at Summit; MERRA = Modern-Era Retrospective Analysis for Research and Applications; CERES = Clouds and the Earth's Radiant Energy System; ASR = Arctic System Reanalysis; LENS = Large ENSemble Community Project.

inadequate low-level cloud definition over Greenland. In LENS, although low-level cloud fraction is important, the strong correlation with ice water path dominates longwave CRE, counter to observations. The cloud-radiation physics in ASR is distinct. Its net CRE exhibits strong correlations with longwave, even in the ablation zones. Although its shortwave CRE positively correlates with albedo, it exhibits no or positive correlations with cloud fractions, opposite to observations. Its longwave CRE strengthens with cloud fraction and low-level cloud fraction in the ablation zones. In the accumulation zones, low-level cloud fraction shows almost no correlation. Instead, water path, especially ice water path, determines longwave.

We evaluate albedo retrievals from the gridded data sets at each AWS using monthly data averaged over 2008–2013 to avoid asymmetrical seasonal cycles caused by missing values (Figure 10). ASR and MERRA-2 agree best with in situ measurements, with the strongest correlations and the lowest root-mean-square difference. Both of them slightly underestimate albedo by ~0.05 and ~0.08, separately. ERA-Interim, CERES, and LENS flatten the variable albedo in the ablation zone to higher values, and this reduces their spatial variability. Moreover, AWS observations may already overestimate albedo by up to 0.1 due to underrepresentation of albedo spatial heterogeneity (Ryan et al., 2017), making albedo from ERA-Interim, CERES, and LENS even higher than the "ground truth."

We now evaluate cloud fraction and LWP from the gridded data sets against data from ICECAPS at Summit. This station provides the only multiyear in situ observation of clouds in Greenland and represents the continental environments in the snow-covered accumulation zone (Shupe, Turner, et al., 2013). Cloud distributions in the coastal areas are more complex, influenced by a mix of surface types (e.g., open water, sea ice, and tundra) and thus variable heat and moisture fluxes and transportation (Neff, 2018; Walsh et al., 2009). During the three melt seasons from 2011 to 2013, CERES is the closest to the ICECAPS observations for both cloud properties, in terms of magnitude and variability (Figure 11). The cloud fraction qualities of MERRA-2, ERA-Interim, and LENS are similar with either relatively consistent magnitudes or variabilities, but not both. ASR overestimates cloud fraction considerably. As for LWP, discrepancies are larger. LENS shows negligible values throughout the whole melt season. MERRA-2 lacks the variability. ERA-Interim and ASR underestimate the magnitude. Most of these features also exist in the comparisons between data sets over Greenland (Figure 12). MERRA-2, ERA-Interim, CERES, and LENS present a similar cloud fraction spatial distribution, with high values centered over Summit and near southwestern and northern coasts. Cloud fraction from the combined CloudSat-CALIPSO-CERES-Moderate Resolution Imaging Spectroradiometer data product also exhibits high values around the Summit area, however higher values spreading to the northwest (Huang et al., 2017). The spatial distribution of liquid-containing cloud fraction from the GCM Oriented CALIPSO Cloud Product (CALIPSO-GOCCP) presents a better agreement (Cesana et al., 2012). The high values of ASR spread along the mountain ridges. It substantially overestimates cloud fraction, with the lowest values close to the averages of others. The LWP spatial distributions are more consistent than cloud fraction and generally increases with elevation. Nevertheless, the low centers shift from Summit in CERES and LENS toward northwest in ERA-Interim and MERRA-2. The spatial distribution in ASR is scattered. CERES has the largest LWP retrievals. MERRA-2 and ERA-Interim are the next. LENS LWP is almost one magnitude smaller than others. Kay et al. (2016) also report the "insufficient" liquid clouds in CESM over the Arctic Ocean, compared with CALIPSO. It is possible that the growth of ice clouds scavenges too much supercooled cloud liquid, predicting insufficient liquid clouds in the polar regions (McIlhattan et al., 2017).

In summary, MERRA-2 captures the major features of cloud-radiation physics and simulates both albedo and cloud properties well, resulting in the best CRE estimates among the five gridded data sets examined here. ERA-Interim and CERES reproduce both good physics and cloud properties. Therefore, they present the same spatial distribution as in situ weather stations, a warm center pattern. The physics of LENS is mostly similar to observations. However, LENS predicts LWP almost one magnitude smaller than in situ measurements.

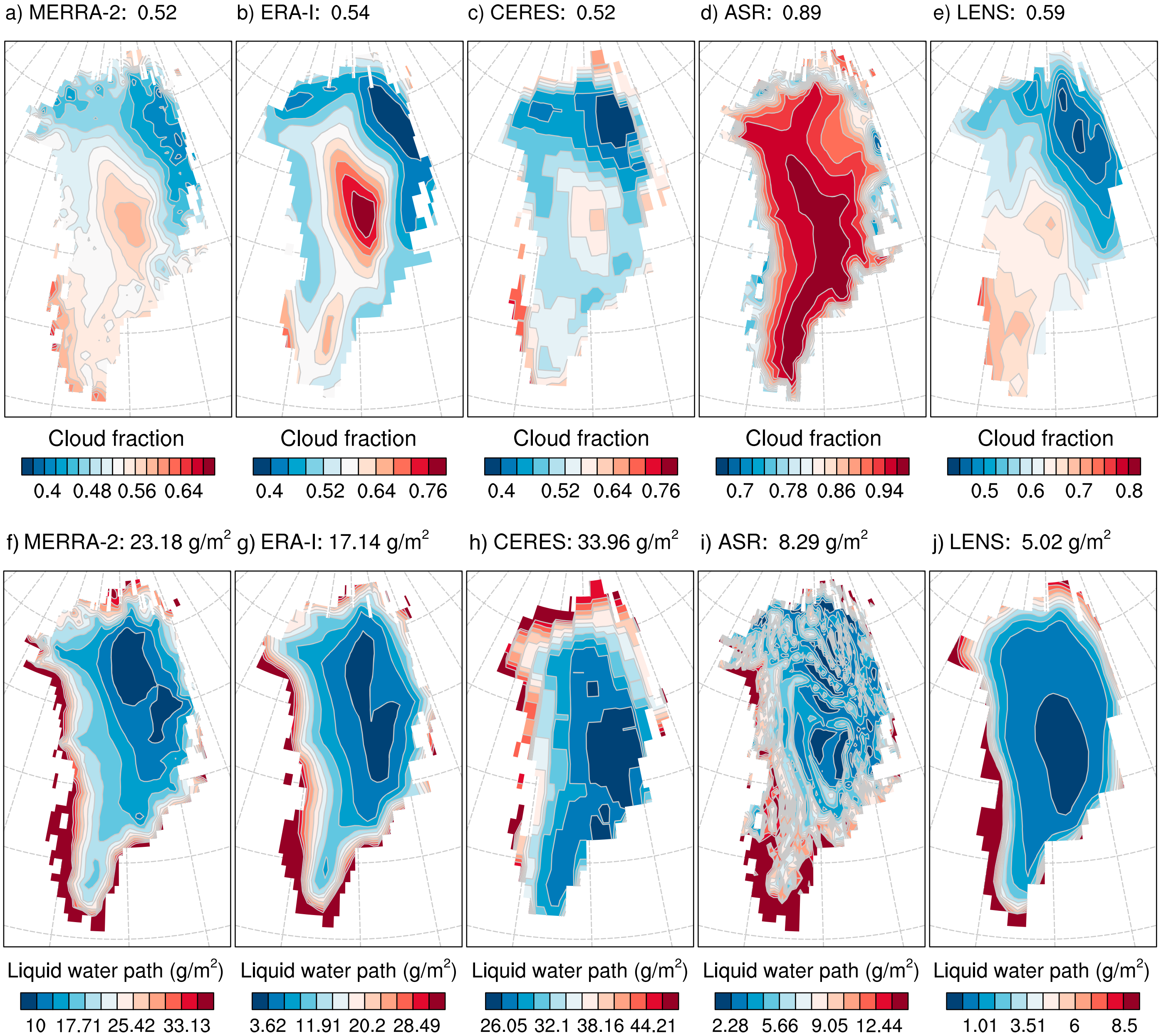

Figure 12. Cloud fraction (a–e) and liquid water path (f–j) from the five gridded data sets (each represented by one column) in melt seasons from 2008 to 2013. Numbers above panels are areal averages. The inter-data set differences are too large to have a common color label. MERRA = Modern-Era Retrospective Analysis for Research and Applications; CERES = Clouds and the Earth's Radiant Energy System; ASR = Arctic System Reanalysis; LENS = Large ENSemble Community Project.

Moreover, due to the favorable response of longwave CRE to ice water path instead of to cloud factions in the accumulation zone, net CRE in LENS presents a warm L-shape spatial distribution (similar to that of ice water path; Figure S3). ASR achieves the best albedo. However, it falsely correlates shortwave CRE and cloud fractions in a positive manner and overestimates cloud fraction substantially, leading to a warm L-shape spatial distribution different from AWS estimates.

6. Discussion: Warm L-Shape CRE Spatial Distribution From CALIPSO

Annual mean CRE estimated using CALIPSO products shows a warm L-shape spatial distribution during 2007–2010 with an areal average of 29.5 W/m^2 (Van Tricht et al., 2016). This annual distribution differs from

10.1029/2018JD028919

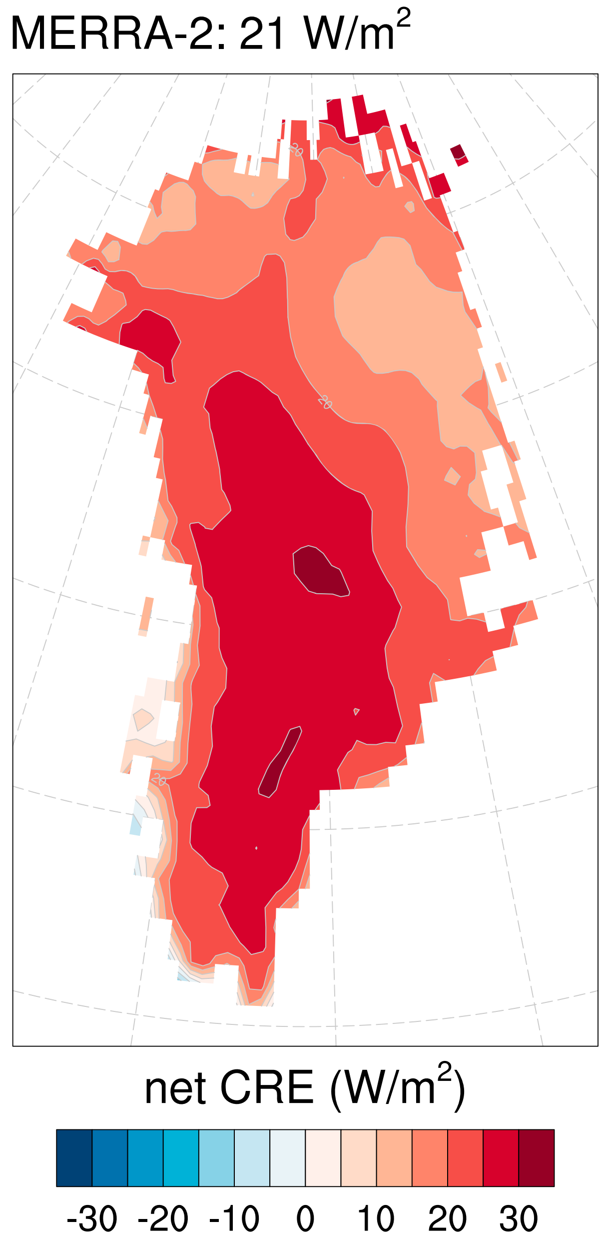

Figure 13. Annual mean CRE from MERRA-2 during 2007–2010. Number above is the areal average. MERRA = Modern-Era Retrospective Analysis for Research and Applications; CRE = cloud radiative effects.

the AWS observed warm center spatial distribution in melt season. In order to preclude the influence of seasonality and interannual variability, we estimate annual mean CRE during the same time period as Van Tricht et al. (2016) using MERRA-2. The annual mean is close (21 W/m^2) considering the large range of CRE (Figure 3). However, MERRA-2 still exhibits a warm center distribution with the only exception in the northern ablation zone (Figure 13). We expect this distribution because in the accumulation zone, longwave CRE and shortwave CRE both decrease with elevation. Therefore, the spatial distributions in winter, when there is only longwave radiation, and in summer, when there are both longwave and shortwave radiation, are similar. In the sunlit southern ablation zone, annual net CRE also decreases with elevation, same as in summer. However, in the northern ablation zone, where there is no sunlight during winter, net CRE (dominated by longwave CRE) increases instead of decreases with elevation toward coasts. As mentioned above, although with active sensors, CALIPSO products reportedly provide more accurate instantaneous cloud observations (e.g., Cesana & Chepfer, 2012; Chan & Comiso, 2013; Henderson et al., 2013; Kay & L'Ecuyer, 2013), their sparse spatiotemporal sampling might hinder the ability to reproduce climatologies (Kay & L'Ecuyer, 2013; Liu, 2015).

7. Summary

We establish the melt season spatial distribution of CRE over Greenland, estimated from 21 in situ AWS. We use these results to evaluate CRE spatial distributions from five data sets including one satellite product, CERES; two global reanalyses, MERRA-2 and ERA-Interim; one regional reanalysis, ASR; and one global climate model, LENS. We also examine the fidelity of the cloud-radiation physics in the gridded data set results and their ability to reproduce major factors that determine CRE in order to understand the inter-data set differences.

For May–August 2008–2013, net CRE peaks near Summit and decreases with elevation to reach a minimum along coasts. This forms a warm center spatial distribution over Greenland. In the accumulation zone, both longwave and shortwave CRE values decline with elevation. In the ablation zone, although longwave CRE strengthens coastward, the larger spatial variability of shortwave CRE causes net CRE to decrease toward coasts. MERRA-2, ERA-Interim, and CERES exhibit a similar warm center CRE spatial distribution to in situ observations. ASR, LENS, and CALIPSO present a warm L-shape spatial distribution with strong warming in the south and northwest. The largest discrepancy between the two patterns occurs in the accumulation zone where inconsistent cloud-radiation physics alter longwave CRE. MERRA-2, ERA-Interim, and CERES reproduce the strong correlations between longwave CRE and cloud fraction in the accumulation zone. In addition to relatively good simulations of cloud fraction, their net CRE warm the center of Greenland the most. On the other hand, ASR and LENS show stronger correlations between longwave CRE and ice water path, which increases from north to south. Moreover, ASR overestimates cloud fraction, and LENS underestimates LWP, resulting in too small spatial variabilities.

We also evaluate CRE from the five data sets at each weather station to better examine shortwave CRE and ablation zones. Due to accurate model physics and simulations of both albedo and cloud properties, MERRA-2 CRE agree the best with in situ measurements, considering both pattern correlation and variability. In all data sets except ASR, albedo dominates shortwave CRE in the ablation zone and in the southern accumulation zone, consistent with AWS. ASR exhibits an incorrect positive correlation between shortwave CRE and cloud fraction, diminishing the influence of albedo, which it reproduces the best.

Our study identifies the actual warm center spatial distribution of CRE over Greenland and highlights the dependence of longwave CRE on cloud fraction and cloud fraction simulation as the most important factors to successfully simulate CRE on large scales. These results provide ground truth to validate satellite retrievals, model simulations, and reanalyses. Compared to passive sensors, active sensors have advantages observing clouds in snow-covered and low-insolation areas. However, due to their sparse spatiotemporal sampling caused by narrow swaths, retrievals from active sensors may not reproduce the correct CRE spatial distribution. The warm center CRE spatial distribution established from AWS, MERRA-2, ERA-Interim, and CERES indicates the role of clouds as a mediator in surface melt over Greenland. Clouds warm the bright and cloudy Summit area the most where surface melt is very scarce. Clouds cool the dark and cloudy coasts, especially in the west, where heavy mass loss occurs.

Acknowledgments
We thanks Michael G. Bosilovich for explaining the details of MERRA-2 cloud retrieval processes and Dennis Shea and Mary Haley for clarifying spatial interpolation methods used by NCAR Command Language (NCL). The GC-Net data were obtained from the Steffen Research Group, the Cooperative Institute for Research in Environmental Sciences (http://cires1.colorado.edu/science/groups/steffen/gcnet/order/admin/station.php). The PROMICE data were obtained from the PROMICE website, collected by the Geological Survey of Denmark and Greenland (GEUS) in collaboration with the (Technical University of Denmark) DTU Space and Asiaq, Greenland Survey (http://www.promice.org/DataDownload.html). The CERES data were obtained from the NASA Langley Research Center Atmospheric Science Data Center (https://ceres-tool.larc.nasa.gov/ord-tool/jsp/SYN1degSelection.jsp). The MERRA-2 data were obtained from the NASA EARTHDATA, provided by the Global Modeling and Assimilation Office (GMAO) from NASA Goddard Space Flight Center (https://disc.sci.gsfc.nasa.gov/daac-bin/FTPSubset2.pl). The ERA-Interim data were obtained from the European Centre for Medium-Range Weather Forecasts (http://apps.ecmwf.int/datasets/data/interim-full-daily/levtype=sfc/). The ASR data were obtained from the National Center for Atmospheric Research/University Corporation for Atmospheric Research (NCAR/UCAR) and Polar Meteorology Group, Byrd Polar Research Center, the Ohio State University (https://rda.ucar.edu/datasets/ds631.0/;DOI:10.5065/D6K072B5). The LENS data were obtained from the Earth System Grid at NCAR (https://www.earthsystemgrid.org/dataset/ucar.cgd.ccsm4.CESM_CAM5_BGC_LE.atm.proc.monthly_ave.html). The ICECAPS data (supported by NSF PLR1303879) were from ftp://ftp1.esrl.noaa.gov/psd3/arctic/summit/radiosonde/processed/. Project supported by NASA ACCESS NNX14AH55A and by DOE ACME DE-SC0012998.

References

AIRS Science Team/Joao Texeira (2013). Aqua AIRS Level 2 Support Retrieval (AIRS+AMSU), version 00 ed., NASA Goddard Earth Science Data and Information Services Center (GES DISC), Greenbelt, MD, USA. https://doi.org/10.5067/AQUA/AIRS/DATA207

Arking, A. (1991). The radiative effects of clouds and their impact on climate. *Bulletin of the American Meteorological Society*, *72*(6), 795–813. https://doi.org/10.1175/1520-0477(1991)072<0795:TREOCA>2.0.CO;2

Bennartz, R., Shupe, M. D., Turner, D. D., Walden, V. P., Steffen, K., Cox, C. J., et al. (2013). July 2012 Greenland melt extent enhanced by low-level liquid clouds. *Nature*, *496*(7443), 83–86. https://doi.org/10.1038/nature12002

Cesana, G., & Chepfer, H. (2012). How well do climate models simulate cloud vertical structure? A comparison between CALIPSO-GOCCP satellite observations and CMIP5 models. *Geophysical Research Letters*, *39*, L20803. https://doi.org/10.1029/2012GL053153

Cesana, G., Kay, J. E., Chepfer, H., English, J. M., & de Boer, G. (2012). Ubiquitous low-level liquid-containing Arctic clouds: New observations and climate model constraints from CALIPSO-GOCCP. *Geophysical Research Letters*, *39*, L20804. https://doi.org/10.1029/2012GL053385

Cesana, G., Waliser, D. E., Jiang, X., & Li, J. L. (2015). Multimodel evaluation of cloud phase transition using satellite and reanalysis data. *Journal of Geophysical Research: Atmospheres*, *120*, 7871–7892. https://doi.org/10.1002/2014JD022932

Chan, M. A., & Comiso, J. C. (2013). Arctic cloud characteristics as derived from MODIS, CALIPSO, and CloudSat. *Journal of Climate*, *26*(10), 3285–3306. https://doi.org/10.1175/JCLI-D-12-00204.1

Cox, C. J., Walden, V. P., Compo, G. P., & Rowe, P. M. (2014). Downwelling longwave flux over Summit, Greenland, 2010–2012: Analysis of surface-based observations and evaluation of ERA-Interim using wavelets. *Journal of Geophysical Research: Atmospheres*, *119*, 12,317–12,337. https://doi.org/10.1002/2014JD021975

Cox, C. J., Walden, V. P., Rowe, P. M., & Shupe, M. D. (2015). Humidity trends imply increased sensitivity to clouds in a warming Arctic. *Nature Communications*, *6*(10), 117. https://doi.org/10.1038/ncomms10117

Curry, J. A., Rossow, W. B., Randall, D., & Schramm, J. L. (1996). Overview of Arctic cloud and radiation characteristics. *Journal of Climate*, *9*(8), 1731–1764. https://doi.org/10.1175/1520-0442(1996)009<1731:OOACAR>2.0.CO;2

Dee, D. P., Uppala, S. M., Simmons, A. J., Berrisford, P., Poli, P., Kobayashi, S., et al. (2011). The ERA-Interim reanalysis: Configuration and performance of the data assimilation system. *Quarterly Journal of the Royal Meteorological Society*, *137*(656), 553–597. https://doi.org/10.1002/qj.828

European Centre for Medium-Range Weather Forecasts (2018). How are low, medium and high cloud cover defined? Retrieved from https://www.ecmwf.int/en/faq/how-are-low-medium-and-high-cloud-cover-defined

Fettweis, X., Box, J. E., Agosta, C., Amory, C., Kittel, C., & Gallée, H. (2017). Reconstructions of the 1900–2015 Greenland ice sheet surface mass balance using the regional climate MAR model. *The Cryosphere*, *11*(2), 1015–1033. https://doi.org/10.5194/tc-2016-268

Geier, E. B., Green, R. N., Kratz, D. P., Minnis, P., Miller, W. F., Nolan, S. K., & Franklin, C. B. (2003). *Clouds and the Earth's Radiant Energy System (CERES) data management system single satellite footprint TOA/surface fluxes and clouds (SSF) collection document* (2nd ed., pp. 1–231). Hampton, VA: Primary Authors Science Directorate Science Applications Internation.

Gelaro, R., McCarty, W., Suárez, M. J., Todling, R., Molod, A., Takacs, L., et al. (2017). The Modern-Era Retrospective Analysis for Research and Applications, version 2 (MERRA-2). *Journal of Climate*, *30*(14), 5419–5454. https://doi.org/10.1175/JCLI-D-16-0758.1

Hall, D. K., Nghiem, S. V., Schaaf, C. B., DiGirolamo, N. E., & Neumann, G. (2009). Evaluation of surface and near-surface melt characteristics on the Greenland ice sheet using MODIS and QuikSCAT data. *Journal of Geophysical Research*, *114*, F04006. https://doi.org/10.1029/2009JF001287

Hanna, E., Fettweis, X., Mernild, S. H., Cappelen, J., Ribergaard, M. H., Shuman, C. A., et al. (2014). Atmospheric and oceanic climate forcing of the exceptional Greenland ice sheet surface melt in summer 2012. *International Journal of Climatology*, *34*(4), 1022–1037. https://doi.org/10.1002/joc.3743

Henderson, D. S., L'Ecuyer, T., Stephens, G., Partain, P., & Sekiguchi, M. (2013). A multisensor perspective on the radiative impacts of clouds and aerosols. *Journal of Applied Meteorology and Climatology*, *52*(4), 853–871. https://doi.org/10.1175/JAMC-D-12-025.1

Hofer, S., Tedstone, A. J., Fettweis, X., & Bamber, J. L. (2017). Decreasing cloud cover drives the recent mass loss on the Greenland Ice Sheet. *Science Advances*, *3*, e1700584. https://doi.org/10.1126/sciadv.1700584

Huang, Y., Dong, X., Xi, B., Dolinar, E. K., Stanfield, R. E., & Qiu, S. (2017). Quantifying the uncertainties of reanalyzed Arctic cloud and radiation properties using satellite surface observations. *Journal of Climate*, *30*(19), 8007–8029. https://doi.org/10.1175/JCLI-D-16-0722.1

Intrieri, J. M., Fairall, C. W., Shupe, M. D., Persson, P. O. G., Andreas, E. L., Guest, P. S., & Moritz, R. E. (2002). An annual cycle of Arctic surface cloud forcing at SHEBA. *Journal of Geophysical Research*, *107*(C10), 8039. https://doi.org/10.1029/2000JC000439

Kay, J. E., Bourdages, L., Miller, N. B., Morrison, A., Yettella, V., Chepfer, H., & Eaton, B. (2016). Evaluating and improving cloud phase in the Community Atmosphere Model version 5 using spaceborne lidar observations. *Journal of Geophysical Research: Atmospheres*, *121*, 4162–4176. https://doi.org/10.1002/2015JD024699

Kay, J. E., Deser, C., Phillips, A., Mai, A., Hannay, C., Strand, G., et al. (2015). The Community Earth System Model (CESM) Large Ensemble Project: A community resource for studying climate change in the presence of internal climate variability. *Bulletin of the American Meteorological Society*, *96*(8), 1333–1349. https://doi.org/10.1175/BAMS-D-13-00255.1

Kay, J. E., & Gettelman, A. (2009). Cloud influence on and response to seasonal Arctic sea ice loss. *Journal of Geophysical Research*, *114*, D18204. https://doi.org/10.1029/2009JD011773

Kay, J. E., & L'Ecuyer, T. (2013). Observational constraints on Arctic Ocean clouds and radiative fluxes during the early 21st century. *Journal of Geophysical Research: Atmospheres*, *118*, 7219–7236. https://doi.org/10.1002/jgrd.50489

Lacour, A., Chepfer, H., Shupe, M. D., Miller, N. B., Noel, V., Kay, J., et al. (2017). Greenland clouds observed in CALIPSO-GOCCP: Comparison with ground-based summit observations. *Journal of Climate*, *30*(15), 6065–6083. https://doi.org/10.1175/JCLI-D-16-0552.1

Li, Z., & Trishchenko, A. (2001). Quantifying uncertainties in determining SW cloud radiative forcing and cloud absorption due to variability in atmospheric conditions. *Journal of the Atmospheric Sciences*, *58*, 376–389. https://doi.org/10.1175/1520-0469(2001)058<0376:QUIDSC>2.0.CO;2

Liu, Y. (2015). Estimating errors in cloud amount and cloud optical thickness due to limited spatial sampling using a satellite imager as a proxy for nadir-view sensors. *Journal of Geophysical Research: Atmospheres*, *120*, 6980–6991. https://doi.org/10.1002/2015JD023507

Liu, Y., & Key, J. R. (2016). Assessment of Arctic cloud cover AnoMalies in atmospheric reanalysis products using satellite data. *Journal of Climate*, *29*, 6065–6083. https://doi.org/10.1175/JCLI-D-15-0861.1

McIlhattan, E. A., L'Ecuyer, T. S., & Miller, N. B. (2017). Observational evidence linking arctic supercooled liquid cloud biases in CESM to snowfall processes. *Journal of Climate*, *30*(12), 4477–4495. https://doi.org/10.1175/JCLI-D-16-0666.1

Miller, N. B., Shupe, M. D., Cox, C. J., Walden, V. P., Turner, D. D., Steffen, K., et al. (2015). Cloud radiative forcing at Summit, Greenland. *Journal of Climate*, *28*(15), 6267–6280. https://doi.org/10.1175/JCLI-D-15-0076.1

Neff, W. (2018). Atmospheric rivers melt Greenland. *Nature Climate Change*, *8*(October), 857–858. https://doi.org/10.1038/s41582-018-0008-9

Noël, B., van de Berg, W. J., van Meijgaard, E., Kuipers Munneke, P., van de Wal, R. S. W., & van den Broeke, M. R. (2015). Evaluation of the updated regional climate model RACMO2.3: Summer snowfall impact on the Greenland Ice Sheet. *The Cryosphere*, *9*(5), 1831–1844. https://doi.org/10.5194/tc-9-1831-2015

Perovich, D. K., Grenfell, T. C., Light, B., & Hobbs, P. V. (2002). Seasonal evolution of the albedo of multiyear Arctic sea ice. *Journal of Geophysical Research*, *107*(C10), 8044. https://doi.org/10.1029/2000JC000438

Qian, Y., Long, C. N., Wang, H., Comstock, J. M., McFarlane, S. A., & Xie, S. (2012). Evaluation of cloud fraction and its radiative effect simulated by IPCC AR4 global models against ARM surface observations. *Atmospheric Chemistry and Physics*, *12*(4), 1785–1810. https://doi.org/10.5194/acp-12-1785-2012

Ryan, J. C., Hubbard, A., Irvine-Fynn, T. D., Doyle, S. H., Cook, J. M., Stibal, M., & Box, J. E. (2017). How robust are in situ observations for validating satellite-derived albedo over the dark zone of the Greenland Ice Sheet? *Geophysical Research Letters*, *44*, 6218–6225. https://doi.org/10.1002/2017GL073661

Sanford, T., Frumhoff, P. C., Luers, A., & Gulledge, J. (2014). The climate policy narrative for a dangerously warming world. *Nature Climate Change*, *4*(3), 164–166. https://doi.org/10.1038/nclimate2148

Shupe, M. D., & Intrieri, J. M. (2004). Cloud radiative forcing of the Arctic surface: The influence of cloud properties, surface albedo, and solar zenith angle. *Journal of Climate*, *17*(3), 616–628. https://doi.org/10.1175/1520-0442(2004)017<0616:CRFOTA>2.0.CO;2

Shupe, M. D., Persson, P. O. G., Brooks, I. M., Tjernström, M., Sedlar, J., Mauritsen, T., et al. (2013). Cloud and boundary layer interactions over the Arctic sea ice in late summer. *Atmospheric Chemistry and Physics*, *13*(18), 9379–9399. https://doi.org/10.5194/acp-13-9379-2013

Shupe, M. D., Turner, D. D., Walden, V. P., Bennartz, R., Cadeddu, M. P., Castellani, B. B., et al. (2013). High and dry: New observations of tropospheric and cloud properties above the Greenland Ice Sheet. *Bulletin of the American Meteorological Society*, *94*(2), 169–186. https://doi.org/10.1175/BAMS-D-11-00249.1

Steffen, C., Box, J., & Abdalati, W. (1996). Greenland Climate Network: GC-Net, US Army Cold Regions Reattach and Engineering (CRREL), CRREL Special Report 98–103 pp.

Tjernström, M., Leck, C., Birch, C. E., Bottenheim, J. W., Brooks, B. J., Brooks, I. M., et al. (2014). The Arctic Summer Cloud Ocean Study (ASCOS): Overview and experimental design. *Atmospheric Chemistry and Physics*, *14*(6), 2823–2869. https://doi.org/10.5194/acp-14-2823-2014

Turner, D. D., Clough, S. A., Liljegren, J. C., Clothiaux, E. E., Cady-Pereira, K. E., & Gaustad, K. L. (2007). Retrieving liquid water path and precipitable water vapor from the Atmospheric Radiation Measurement (ARM) microwave radiometers. *IEEE Transactions on Geoscience and Remote Sensing*, *45*(11), 3680–3690. https://doi.org/10.1109/TGRS.2007.903703

van As, D., & Fausto, R. S. (2011). the PROMICE project team Programme for Monitoring of the Greenland Ice Sheet (PROMICE): First temperature and ablation records. *Geological Survey of Denmark and Greenland Bulletin*, *23*, 73–76.

Van Tricht, K., Lhermitte, S., Lenaerts, J. T. M., Gorodetskaya, I. V., L'Ecuyer, T. S., Noël, B., et al. (2016). Clouds enhance Greenland ice sheet meltwater runoff. *Nature Communications*, *7*(10), 266. https://doi.org/10.1038/ncomms10266

Verlinde, J., Zak, B. D., Shupe, M. D., Ivey, M. D., & Stamnes, K. (2016). The ARM north dlope of Alaska (NSA) sites. In D. D. Turner & R. G. Ellingson (Eds.), *The Atmospheric Radiation Measurement (ARM) program: The first 20 years. Meteorological Monographs* (Chap. 8, Vol. 57, pp. 8.1–8.13). Chicago, Ill: American Meteorological Society. https://doi.org/10.1175/AMSMONOGRAPHS-D-15-0023.1

Walsh, J. E., Chapman, W. L., & Portis, D. H. (2009). Arctic cloud fraction and radiative fluxes in atmospheric reanalyses. *Journal of Climate*, *22*(9), 2316–2334. https://doi.org/10.1175/2008JCLI2213.1

Wang, W., Zender, C. S., & van As, D. (2018). Temporal characteristics of cloud radiative effects on the greenland ice sheet: Discoveries from multiyear automatic weather station measurements. *Journal of Geophysical Research: Atmospheres*, *123*, 11,348–11,361. https://doi.org/10.1029/2018JD028540

Wang, W., Zender, C. S., van As, D., Smeets, P. C. J. P., & van den Broeke, M. R. (2016). A Retrospective, Iterative, Geometry-Based (RIGB) tilt-correction method for radiation observed by automatic weather stations on snow-covered surfaces: Application to Greenland. *The Cryosphere*, *10*(2), 727–741. https://doi.org/10.5194/tc-10-727-2016

Wesslén, C., Tjernström, M., Bromwich, D. H., de Boer, G., Ekman, A. M. L., Bai, L.-S., & Wang, S.-H. (2014). The Arctic summer atmosphere: An evaluation of reanalyses using ASCOS data. *Atmospheric Chemistry and Physics*, *14*(5), 2605–2624. https://doi.org/10.5194/acp-14-2605-2014

Wielicki, B. A., Barkstrom, B. R., Harrison, E. F., Lee, R. B., Smith, G. L., & Cooper, J. E. (1996). Clouds and the Earth's Radiant Energy System (CERES): An Earth observing system experiment. *Bulletin of the American Meteorological Society*, *77*, 853–868. https://doi.org/10.1175/1520-0477(1996)077<0853:CATERE>2.0.CO;2

Zender, C. S. (1999). Global climatology of abundance and solar absorption of oxygen collision complexes. *Journal of Geophysical Research*, *104*(D20), 24–471. https://doi.org/10.1029/1999JD900797

Zib, B. J., Dong, X., Xi, B., & Kennedy, A. (2012). Evaluation and intercomparison of cloud fraction and radiative fluxes in recent reanalyses over the Arctic using BSRN surface observations. *Journal of Climate*, *25*(7), 2291–2305. https://doi.org/10.1175/JCLI-D-11-00147.1

Zygmuntowska, M., Mauritsen, T., Quaas, J., & Kaleschke, L. (2012). Arctic clouds and surface radiation—A critical comparison of satellite retrievals and the ERA-Interim reanalysis. *Atmospheric Chemistry and Physics*, *12*(14), 6667–6677. https://doi.org/10.5194/acp-12-6667-2012